Nanoscale Research Letters

NANO EXPRESS

Open Access

$CoFe_2O_4$-Quantum Dots for Synergistic Photothermal/Photodynamic Therapy of Non-small-Cell Lung Cancer Via Triggering Apoptosis by Regulating PI3K/AKT Pathway

Jingfeng Liu[1,2], Xiaoying Shi[3], Rongjun Zhang[4], Miaomiao Zhang[1,2], Juan He[1,2], Jian Chen[1,2*], Zheng Wang[5*] and Qingwen Wang[1,2*]

Abstract

Non-small-cell lung cancer (NSCLC) has become the second most diagnosed malignant tumors worldwide. As our long-term interests in seeking nanomaterials to develop strategies of cancer therapies, we herein constructed novel $CoFe_2O_4$-quantum dots (QDs) with outstanding synergistic photothermal/photodynamic property which suppressed NSCLC efficiently without apparent toxicity. We showed that the combination of $CoFe_2O_4$-QDs + NIR treatment induces apoptosis of NSCLC cells. In addition, the $CoFe_2O_4$-QDs + NIR treatment also promotes reactive oxygen species generation to trigger cell death through regulating PI3K/AKT pathway. Moreover, the $CoFe_2O_4$-QDs + NIR treatment successfully eliminates tumor xenografts in vivo without apparent toxic effects. Taken together, we reported that the novel nanomaterials $CoFe_2O_4$-QDs could exhibit enhanced synergistic photothermal therapy and photodynamic therapy effect on killing NSCLC without toxicity, which could be a promising photosensitizer for NSCLC therapy.

Keywords: Quantum Dots, NSCLC, Photodymatic therapy, ROS, PI3K/Akt

Introduction

Cancer is the leading cause of death and brings huge burden for the family and society, among which lung cancer ranks the second most diagnosed cancer and the first of cancer-related death in 2020 [1, 2]. As reported, non-small-cell lung cancer (NSCLC), which accounts about 85% of all lung cancers, is characterized in high incidence and mortality [3, 4]. Recently, in spite of surgical options, great effort has been given to develop chemotherapies or immunotherapies to treat NSCLC. For example, EGFR-mutant inhibitors and KRAS inhibitors have been proved effective and there still more novel ALK inhibitors are ongoing [5–9]. Anti-PDL1 and anti-CLTA4, such immune check point inhibitors also bring promising efficacy and prolong survival benefit [10–12]. However, the responsive rate toward these drugs differs from patient to patient and the side effects, especially drug resistance, should not be neglected [13, 14]. Therefore, to develop novel therapeutic strategies, which are less invasive, is an urgent and also a necessity for NSCLC research and clinical treatments.

Based on recent progress, using nanomaterials to perform photothermal therapy (PTT) and photodynamic therapy (PDT) has aroused tremendous attention and reached great development as an anti-cancer strategy and may be an alternative option in clinical treatment [15–18]. Nanomaterial-based PTT and PDT is characterized

*Correspondence: chenjian@jnu.edu.cn; zhengwang@xidian.edu.cn; wqw_sw@163.com
[1] Department of Rheumatism and Immunology, Peking University Shenzhen Hospital, Shenzhen Peking University-The Hong Kong University of Science and Technology Medical Center, Shenzhen 518036, Guangdong, China
[5] School of Advanced Materials and Nanotechnology, Xidian University, Xi'an 710126, China
Full list of author information is available at the end of the article

in less invasion and low toxicity, which with little chance to induce drug resistance [19–23]. With the collaboration of light, mostly NIR, localized nanomaterials can raise the temperature within the tumor and convert oxygen to cytotoxicity reactive oxygen species (ROS), which causes cell death in order to eliminate tumors [24]. In this context, the nanomaterial plays a key role in here to influence the efficacy and guarantee the safety. Although such nanomaterials have included metal nanostructures [25], carbon-based materials [26, 27], polymeric nanoparticles (PNPs) [28] or semiconductor compounds [29], they have their own limitations. For example, carbon-based materials are costly and have unsatisfactory suspension property, which limits its application in large scale and clinical potentiality. Therefore, more attempts should be addressed to generate more suitable nanomaterials for further usage.

Recent years, quantum dots (QDs), as novel nanomaterials, have received great attraction in biomedical applications because of their good bio-compatibility, solubility and the most important their superior photostability and facile surface functionalization property [30–33]. Taking advantage of these properties, several reports have used QDs as novel PDT reagents and can be designed to be accompanied with other biomolecules to enhance the efficacy of PDT in cancer treatment. For example, Meng and colleagues reported a multi-functional GQD@MnO_2 induced by two-photo excitation to improve the PDT efficacy [34]. In addition, Kuo and colleagues generated nitrogen-doped QDs by functionalized them with amino molecules, which enhanced the PDT efficiency as well [35]. Inspired by these interesting findings, we sought to develop novel QDs combined with non-noble metal-based nanomaterial which may bring PTT and PDT synergistic effects in one nano-system. For example, Co-based nanomaterial is well-studied non-noble metal-based nanomaterial, which is known for used as PTT agents for tumor therapy or imaging [36]. Therefore, we suggested that designing Co-based QDs may bring enhanced PTT/PDT synergistic effects.

In this study, we synthesized novel nanomaterials $CoFe_2O_4$-QDs which exhibits enhanced PTT and PDT synergistic effects on killing NSCLC without toxic effects in vitro and in vivo, which could be a promising photosensitizer for NSCLC therapy.

Table1 Reagents or resource used in this study

Reagents or resource	Source	Identifier
$CoCl_2{\cdot}6H_2O$	Sigma-Aldrich	Cat# 255599
$Fe(NO_3)_3{\cdot}9H_2O$	Sigma-Aldrich	Cat# 216828
Propylene glycol	Sigma-Aldrich	Cat# 398039
RPMI-1640	Gibco	Cat# 11875119
Fetal bovine serum (FBS)	Gibco	Cat# 10270106
Penicillin–Streptomycin	Gibco	Cat# 15140122
Endothelial cell growth medium	Sigma-Aldrich	Cat# 211–500
CCK-8 Kit	Dojindo	Cat# CK04-05
Annexin-V/PI apoptosis kit	BD Bioscience	Cat# 556547
DCFH-DA	Abcam	Cat# ab113851
NAC inhibitor	Sigma-Aldrich	Cat# A7250
RIPA lysis buffer	Thermo Fisher	Cat# 89900
MatriGel	Corning	Cat# 354277

Material and Methods

Synthesis of $CoFe_2O_4$-QDs

The $CoFe_2O_4$-QDs were synthesized though hydrothermal method. Typically, 0.238 g $CoCl_2{\cdot}6H_2O$ and 0.808 g $Fe(NO_3)_3{\cdot}9H_2O$ were dissolved in 10 mL H_2O and 10 mL propylene glycol mixture solvent, and then stirred for 10 min. Then 4 mL dithranol amine was added into the solution drop by drop, followed by stirring for 30 min. Then the obtained slurry was transformed to a 50 mL stainless Teflon-lined autoclave. The autoclave was maintained at 160 ℃ for 3 h in an oven. The $CoFe_2O_4$-QDs were collected by centrifuging at 8500 rpm for 10 min and then rinsed by deionized water and ethanol successively. Reagents and materials used in this study could be found in Table 1.

Characterization of $CoFe_2O_4$-QDs

The morphology and size of prepared $CoFe_2O_4$-QDs were determined by TEM and EDS system. The crystal structure was analyzed by X-ray diffractometer (Bruker Germany) equipped with Cu Ka radiation ($k = 0.15406$ nm). The absorbance spectrum of $CoFe_2O_4$-QDs was detected by SHIMADZU UV-2600 spectrophotometer. The element valence states of $CoFe_2O_4$-QDs were determined by X-ray photoemission spectroscopy measurements (XPS, VG ESCALAB 220I-XL, USA). The thermal image was recorded with IR thermal camera (FLIR E50, USA).

Cell Culture

NSCLC cell line NCI-H460 (H460) and A549 and Human umbilical vein endothelial cells (HUVECs) were obtained from ATCC and tested for micro-plasma negative. H460 and A549 cells were cultured in RPMI-1640 supplemented with 10% fetal bovine serum (FBS) and 1% Penicillin–Streptomycin (Gibco). HUVECs were cultured in endothelial cell growth medium (Sigma, #211-500). All the cells were kept in dark humidity 37 ℃ incubator with 5% CO_2.

Cytotoxicity Detection

Various working concentrations (0.1, 0.5, 1.0, 2.0 mg/mL) of $CoFe_2O_4$-QDs were added and cultured with HUVECs for 24 h. After incubation, culture medium was changed and CCK-8 regent was added to each well followed by 1 h incubation. Then, plates were measured at 450 nm with EnSpire™ Multimode Plate Reader. The ratio of cell viability was taken as 100% in control HUVECs.

Apoptosis Analysis

H460 and A549 cells (2×10^5) were cultured in 6-well plates overnight before treated with 1.0 mg/mL $CoFe_2O_4$-QDs combined with NIR laser of 808 nm for 5 min. Then cells were washed and stained with Annexin-V/PI apoptosis kit (BD; #556547) following manufacturer's instructions. As for HUVECs apoptosis assay, HUVECs were incubated with different concentration of $CoFe_2O_4$-QDs. The apoptosis ratio was determined as described above.

Cellular ROS Detection

H460 and A549 cells were cultured in 6-well plates overnight. Cells were incubated with or without 1.0 mg/mL for 1 h and treated with NIR laser of 808 nm for 5 min. After treatments, DCFH-DA was added and incubated for 30 min followed by FACS detection with excitation/emission at 485 nm/535 nm. As for ROS inhibition assay, ROS inhibitor NAC (Sigma; A7250) was added according to manufacturer's instruction. Data were further quantified with Flow-jo software.

Western Blot Analysis

H460 and A549 cells were treated as apoptosis assay, and the whole cell protein was extracted using RIPA lysis buffer. Western blot detection was carried out as described before [37]. The antibodies used in this study were listed below: rabbit polyclonal anti-Bcl-2 (abcam; ab59348), rabbit monoclonal anti-Bax (abcam; ab32503), rabbit polyclonal anti-*P*-PI3K (Bio-Vision; 3152-100), rabbit monoclonal anti-*P*-AKT-S473 (CST; 4060S), rabbit monoclonal anti-β-Actin (CST; 4970S), anti-rabbit IgG HRP-linked antibody (CST; 7074S). Quantification was determined by using Image-J software.

In vivo Study of Anti-NSCLC Effect of the Combination of $CoFe_2O_4$ and NIR Treatment

To determine the tumor killing ability of $CoFe_2O_4$-QDs, H460 cells were subcutaneously implanted with 50% MatriGel into NSG mice ($N = 8$ each group). 4–6-week-old male M-NSG mice were obtained from Shanghai Model Organisms (#NM-NSG-001) for all the in vivo experiments. When the tumor was visualized and the volume reached nearly 5 mm × 5 mm, all the mice were randomly divided into four groups, named as Control, NIR only, $CoFe_2O_4$-QDs only and $CoFe_2O_4$-QDs + NIR group, respectively. Then mice in $CoFe_2O_4$-QDs only and $CoFe_2O_4$-QDs + NIR group were intratumorally injected with 50 μL of $CoFe_2O_4$ (5.0 mg/kg) based on our previous work [37], while Control and NIR group was injected with 50 μL of PBS. After injection, NIR 808 nm laser (1 W/cm^2) was performed in NIR and $CoFe_2O_4$-QDs + NIR group for 10 min, which was monitored by infrared thermal imaging equipment. Tumor volume was recorded every day and calculated with the formula $V = \text{length} \times \text{width}^2/2$. Once the diameter of tumor xenografts in remaining mice reached almost 15 mm, mice were sacrificed and tumor xenografts were photographed and stored for further detection. All the animal experiments and protocols were approved by Institutional Animal Care and Use Committee (IACUC) and Animal Welfare Committee of Peking University Shenzhen Hospital.

H&E and Immunohistopathology Staining Analysis

For pathological assessment, the tumor xenografts ($N = 3$) were harvested one day after treatment in each group and then fixed in 10% buffered formalin following embedded in paraffin for H&E staining and IHC detection. For in vivo toxicity evaluation, the kidney, liver, lung, heart and spleen of the mice were extracted and fixed for pathological assessment. For IHC staining, anti-Ki67 antibody (Abcam; ab15580) was used. Quantification of IHC positive area was conducted by software Fiji.

Statistical Analysis

For all experiments, "*N*" represents the number of repeated times or the number of mice used as indicated in the figure legend. Student's *t*-test or one-way ANOVA was used for statistical comparisons. $P < 0.05$ is considered statistically significant while "ns" displays non-significant. $P < 0.05$, $P < 0.01$ and $P < 0.001$ are indicated with "*", "**" and "***" asterisks, respectively. Data were analyzed using GraphPad Prism 5.

Results

The Characteristics of Novel $CoFe_2O_4$-QDs

Firstly, we constructed the $CoFe_2O_4$-QDs using hydrothermal approach which is low cost and simple to perform. The TEM image of $CoFe_2O_4$-QDs was shown in Fig. 1a, presenting a uniform and stable pattern with the diameter around 3.4 nm (Fig. 1b). The as-prepared $CoFe_2O_4$-QDs were dark brown in color (Fig. 1b) and with excellent solubility in water. Furthermore, the high-resolution TEM image (Fig. 1c) displayed the lattice spacing of (222) is about 0.242 nm which is consistent with the crystal parameters of $CoFe_2O_4$-QDs [38, 39]. In addition, the element spectrum (Fig. 1d) further confirmed the element component of the $CoFe_2O_4$-QDs is Co and Fe, and the atom ratio of Co and Fe was about 1:2. These

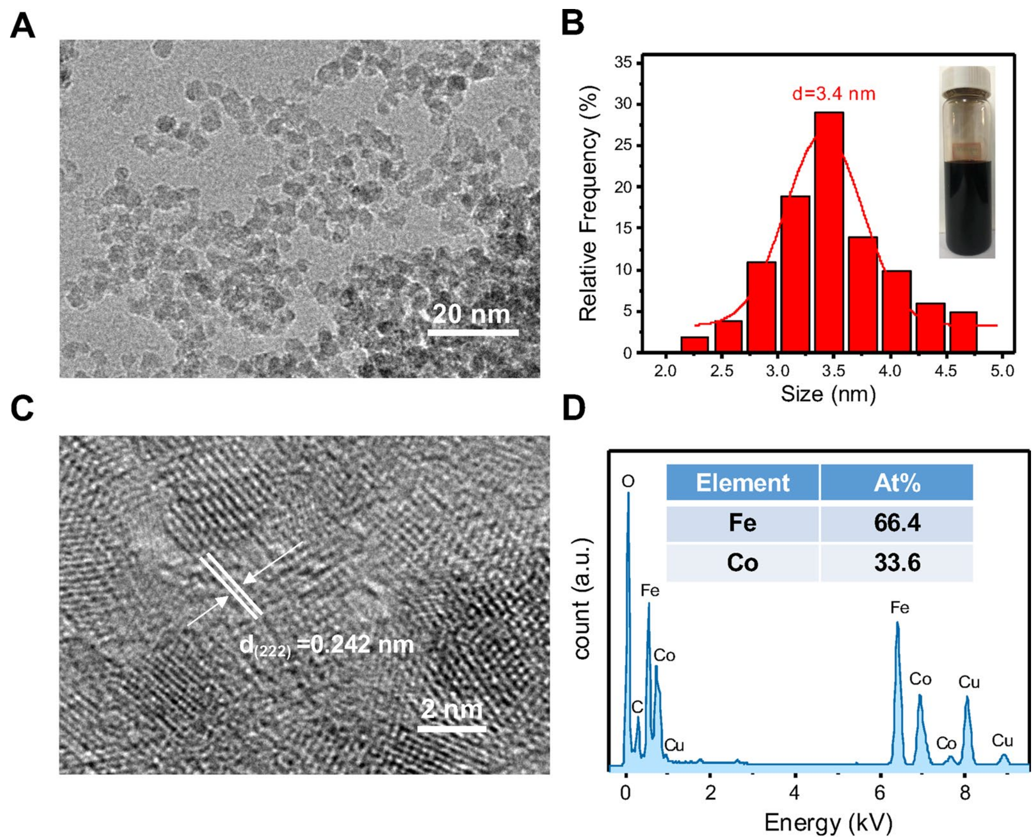

Fig. 1 Preparation and characterization of $CoFe_2O_4$-QDs. **a** The representative TEM image of as-prepared $CoFe_2O_4$-QDs. Scale bar, 20 nm. **b** A global analysis of the size of $CoFe_2O_4$-QDs with the average diameter 3.4 nm. The inset is the representative digital photo of the $CoFe_2O_4$-QDs suspension. **c** The lattice fringes of as-prepared nanocrystals correspond to $CoFe_2O_4$-QDs HRTEM image. Scale bar, 2 nm. **d** The as-prepared $CoFe_2O_4$-QDs exhibited uniform distribution of Co, Fe and O. The representative elements map was shown

data displayed a successful construction of $CoFe_2O_4$-QDs for our further research.

The Physical Property Detection of $CoFe_2O_4$-QDs

In order to determine the physical properties of prepared $CoFe_2O_4$-QDs, we performed several detections after construction. With the NIR absorbance determination test, $CoFe_2O_4$-QDs showed proper photothermal conversion in a concentration dependent manner and the temperature increments (ΔT) could be adjusted from 0.3 to 18.9 °C (Fig. 2a). In addition, at the concentration 1.0 mg/mL of $CoFe_2O_4$-QDs, by increasing the NIR radiation power from 0.5 to 2.0 W/cm^2, the ΔT could be tuned from 0.8 to 24.3 °C (Fig. 2b). These data suggested that the photothermal conversion performance of $CoFe_2O_4$-QDs was dependent on its concentration and the irradiation power. Furthermore, the stability of $CoFe_2O_4$-QDs triggered photothermal conversion was determined with period irradiation (Fig. 2c). Although the calculated light-to-heat conversion efficiency was 7.18% (Fig. 2d), it's enough to be accompanied to enhance the PDT effect of $CoFe_2O_4$-QDs. Moreover, the longest wavelength of $CoFe_2O_4$-QDs can absorb light is about 808 nm (Fig. 2e, f). Taken together, these data suggested that $CoFe_2O_4$-QDs could be developed into a promising PTT/PDT synergistic agent for alternative tumor killing therapy.

Cytotoxicity Assessment of $CoFe_2O_4$-QDs Toward Normal Cells

Since nanoparticles are widely used as drug delivers or intra-medium for tumor therapies, the cytotoxicity of $CoFe_2O_4$-QDs toward normal cells especially human vascular epithelial cells should be confirmed for further usage. Therefore, from the previous results, we tested different concentrations (0.1, 0.5, 1.0 and 2.0 mg/mL) of $CoFe_2O_4$-QDs. After co-cultured with HUVECs (normal human epithelial cell line), CCK-8 reagent was added for the detection of cell viability. There was no obvious cytotoxicity observed comparing to control group (Fig. 3a). In this context, further apoptosis assay was performed to achieve consistent

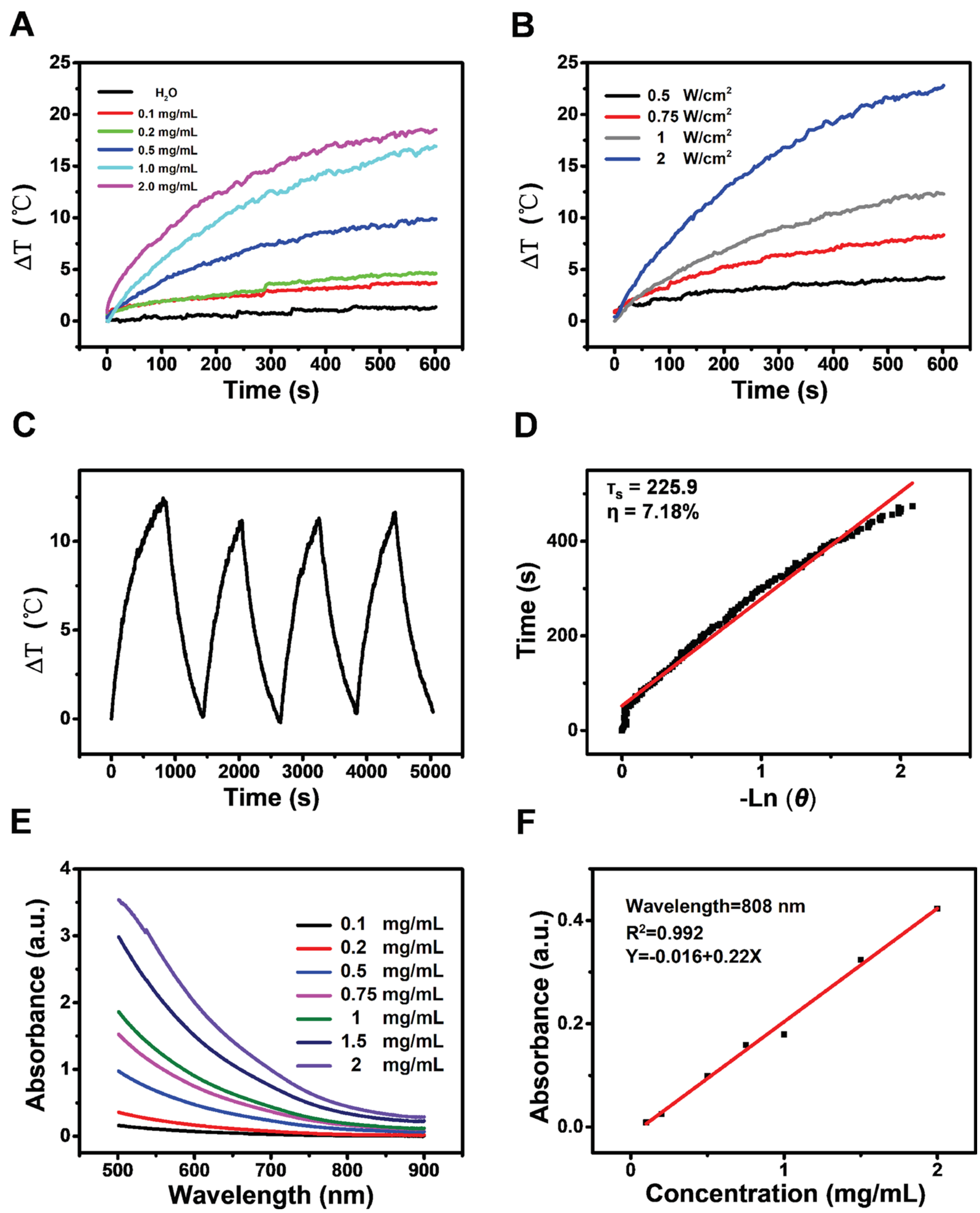

Fig. 2 The property evaluation of $CoFe_2O_4$-QDs. **a** The photothermal conversion of $CoFe_2O_4$-QDs was determined under different concentrations. The heating curves are shown. **b** The irradiation energy dependent manner of $CoFe_2O_4$-QDs is shown at different power densities (0.5–2.0 W/cm^2). **c** $CoFe_2O_4$-QDs have stable photothermal conversion detected with 4 cycles of heating-cooling continuous irradiation (1.0 W/cm^2). **d** The efficiency of $CoFe_2O_4$-QDs photothermal conversion. **e**, **f** The relationship of wavelength and absorbance of $CoFe_2O_4$-QDs

results with the same conditions (Fig. 3b). The quantification of apoptosis rate indicated no significant difference comparing to control group (Fig. 3c). These data showed that $CoFe_2O_4$-QDs had no apparent toxic effect on normal cells, which indicated that $CoFe_2O_4$-QDs had the potential to be used as intermedium for drug deliver.

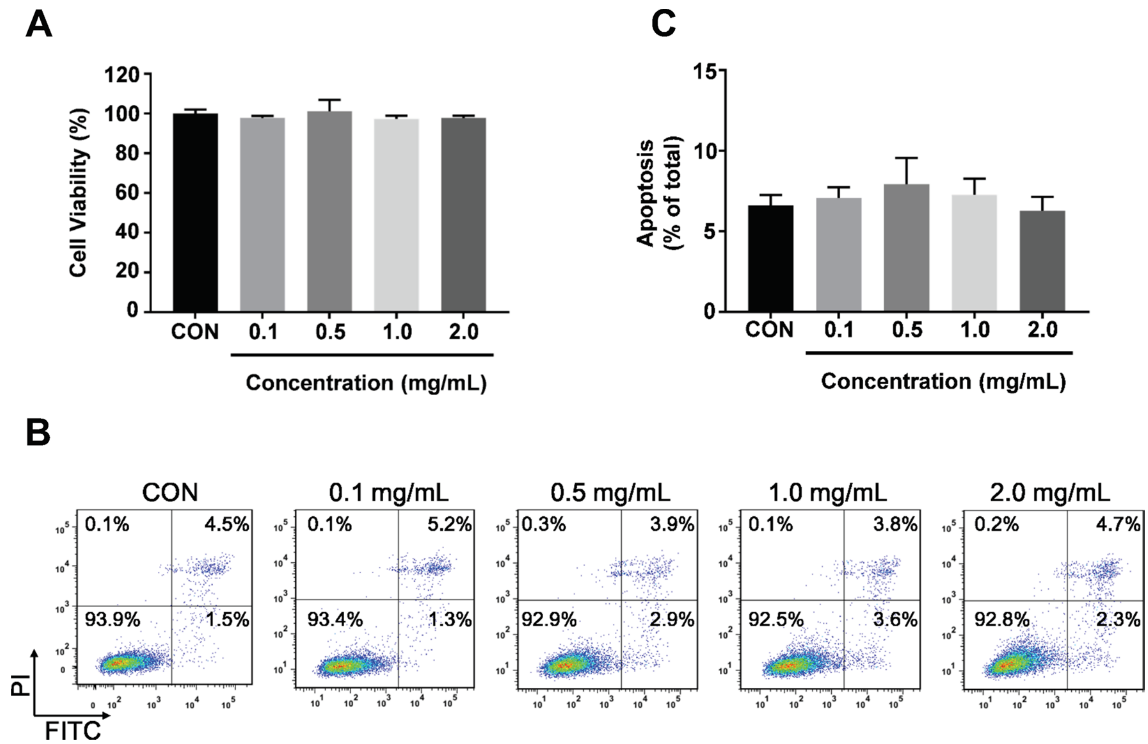

Fig. 3 In vitro assessment of cytotoxicity of $CoFe_2O_4$-QDs toward normal cells. **a** CCK-8 cell viability assay in HUVECs was performed under different concentrations of $CoFe_2O_4$-QDs. The viability of control group was taken as 100%. The data were shown as mean ± SD, $N=3$. **b** HUVECs apoptosis was determined by FACS detection. Representative images of indicated concentrations are shown, $N=3$. **c** The quantification of apoptosis ratio. They show non-significance comparing to control group. The data were shown as mean ± SD

Combination of NIR and $CoFe_2O_4$-QDs Induces Apoptosis of NSCLC

To determine the potential NSCLC cancer killing ability of $CoFe_2O_4$-QDs, NIR laser (808 nm) irradiation was performed combined with incubation of $CoFe_2O_4$-QDs in vitro. Then, apoptosis assay was carried out after treatments, both H460 and A549 cells revealed aggressive apoptosis rate with the combination of $CoFe_2O_4$-QDs and NIR laser (Fig. 4a, b). Quantification showed significant difference comparing to control group, while $CoFe_2O_4$-QDs only or NIR only groups showed no difference which indicated that $CoFe_2O_4$-QDs plus NIR could induce anti-NSCLC effect (Fig. 4a, b). It is well known that the alteration of the protein level of Bcl-2/Bax is important to determine whether the cells would undergo apoptosis [40]. Consistent with this idea, the protein level of Bcl-2 and Bax was determined in both H460 and A549 cells after treatments (Fig. 4c, d). As respected, the data also showed that the ratio of Bcl-2/Bax decreased, which was regarded as the marker of mitochondria-mediated apoptosis. Therefore, we presented that $CoFe_2O_4$-QDs plus NIR gives rise to anti-NSCLC effect through activating mitochondria-mediated apoptosis pathway.

Combination of $CoFe_2O_4$-QDs and NIR Induces ROS Generation via PI3K/AKT Pathway

Mitochondria dysfunction always leads to upregulated level of ROS generation, which cause cell death in NSCLC. In this context, we performed ROS detection after $CoFe_2O_4$-QDs plus NIR treatment in H460 and A549 cells. The results showed that an immense releasing of ROS in combination group, which indicated enhanced PDT effect could be induced by $CoFe_2O_4$-QDs even with low photothermal transmission efficiency (Additional file 1: Fig. S1A, B). Furthermore, the related protein level of PI3K/AKT signaling pathway was also reduced, which suggested that the alteration of ROS was regulated by PI3K/AKT pathway, which leads to the alteration of Bcl-2/Bax protein expression level (Fig. 4c, d, Additional file 1: Fig. S1C, D). To confirm this idea, the ROS inhibitor NAC was added to reverse the phenomenon (Fig. 5a, b). Then, the expression of PI3K/AKT was determined to be rescued after NAC treatment, which further confirmed that the ROS releasing after $CoFe_2O_4$-QDs plus NIR treatment was regulated by PI3K/AKT pathway (Fig. 5c, d). These findings strongly support the idea that the combination of $CoFe_2O_4$-QDs and NIR can lead to synergistic

(See figure on next page.)

Fig. 4 In vitro combination of $CoFe_2O_4$-QDs and NIR induces NSCLC apoptosis. **a**, **b** H460 and A549 NSCLCs were treated with the combination of $CoFe_2O_4$-QDs and NIR laser for 5 min. The apoptotic cells were evaluated by Annexin-V staining and detected by FACS. Quantification is shown respectively as well. The data were shown as mean ± SD, $N=3$. $^{**}P<0.01$ vs Control, NIR, $CoFe_2O_4$ groups. **c**, **d** The protein level of Bcl-2 and Bax were determined by Western blot analysis in NCI-H460 and A549 NSCLC after treatment. Representative images are shown. The quantification is shown after calibrating to the expression of internal control β-Actin. The data were shown as mean ± SD, $N=3$. $^{*}P<0.05$ vs Control, NIR, $CoFe_2O_4$ groups

PTT and PDT effect in killing NSCLC cells by inducing mitochondria dysfunction (ROS) dependent apoptosis.

In vivo Anti-NSCLC Assessment of Combination of $CoFe_2O_4$-QDs and NIR

Based on the in vitro results, we next investigated the anti-NSCLC effect of $CoFe_2O_4$-QDs and NIR combination treatment on NSCLC tumor bearing mice model. M-NSG mice were subcutaneously implanted with H460 cells. After intratumorally injected with $CoFe_2O_4$-QDs, the NIR laser irradiation caused a rapid temperature raise to around 56 °C under the monitor of thermal detection equipment (Fig. 6a, b). Moreover, histopathological staining showed extensive necrosis area observed in combination group indicating that $CoFe_2O_4$-QDs plus NIR treatment caused tumor cell death as a result of tumor elimination (Fig. 6c, d). Further IHC staining also showed that Ki-67 positive area was aggressively shrunk comparing to other groups after the combinational treatment indicating the treated tumor xenografts could no longer proliferate (Additional file 2: Fig. S2A, B). Next, we followed up for 12 days after $CoFe_2O_4$-QDs and NIR treatment. As we expected, the size and weight of the tumor xenografts in other groups remarkedly grow but not in the $CoFe_2O_4$-QDs and NIR treatment group (Fig. 6e, f), supporting the idea that $CoFe_2O_4$-QDs and NIR combined treatment could completely eliminate the tumor xenografts in vivo. As for the cytotoxic effect of $CoFe_2O_4$-QDs, at least in our observation period, no obvious adverse effect was detected from the results of histopathology analysis within important organs of mice (Additional file 2: Fig. S2C). The above data provided strong evidence that $CoFe_2O_4$-QDs could be developed as a novel PTT/PDT reagent for NSCLC treatment.

Discussion

In recent years, the research of developing anti-NSCLC strategies has achieved tremendous progresses. Both the precision medicine targeting specific mutant oncogene-addicted NSCLC and immune checkpoint blockade therapies bring promising future in clinical treatments [41, 42]. However, given the complexity and heterogenicity of tumor microenvironment and underlying risk of losing tumor antigen, it remains a bottleneck to lower the drug resistance rate following the immune evasive status, which leads to tumor relapse in a short time. Therefore, seeking novel treatments or intermedia for NSCLC therapies is an urgent. Among the emerging approaches, nanomaterials have been valued and listed front as effective cancer killing agents. Taking advantages of their small size, good biocompatibilities and thermal transmission abilities, several nanomaterials exert excellent cancer killing abilities in recent researches [43].

In our study, we developed a novel $CoFe_2O_4$-QDs which could be applied as an intermedia for NSCLC treatments via inducing tumor cells apoptosis with synergistic PTT and PDT effects. Like other nanomaterials, $CoFe_2O_4$-QDs exhibited excellent biocompatibilities in our studies which showed no obvious toxicity toward normal cells and major organs. Although we found the thermal transmission rate is not high as other nanomaterials, it's enough for $CoFe_2O_4$-QDs to induce cancer cell apoptosis under the NIR laser activation. $CoFe_2O_4$-QDs shows good linear relationship with the light absorbance in this study and potentially generate ROS with the combination of NIR laser, which further prove that $CoFe_2O_4$-QDs can act as advantaged photosensitizer. We next can further optimize the structure or add thermal sensitive elements to $CoFe_2O_4$-QDs which could reach a higher thermal transmission rate for better synergistic PTT and PDT effects [44, 45]. Moreover, applying chemical drugs or antibodies on the surface of $CoFe_2O_4$-QDs is also feasible, which may bring superior killing efficiency. For example, the approach of linking anti-PDL1 or anti-CTLA4 antibodies to $CoFe_2O_4$-QDs could be a promising combinational therapy in breaking immune suppressive microenvironment within tumors which is our next interests to make a full usage with $CoFe_2O_4$-QDs.

Besides, the mechanism of $CoFe_2O_4$-QDs in killing NSCLC was also elucidated in this study. We confirmed that $CoFe_2O_4$-QDs induced NSCLC apoptosis mainly through ROS secretion after NIR laser activated synergistic PDT and PTT effects. Excess ROS generation causes oxidative stress of tumor cells and directly cause DNA damage, which in turn activate downstream signaling pathways, and then induce death of tumor cells [46, 47]. Among of which, increasing evidence has shown that PI3K/AKT pathway could be regulated by cellular ROS and leads to mitochondria dysfunction [48, 49]. It has been well accepted that upon activation, AKT is

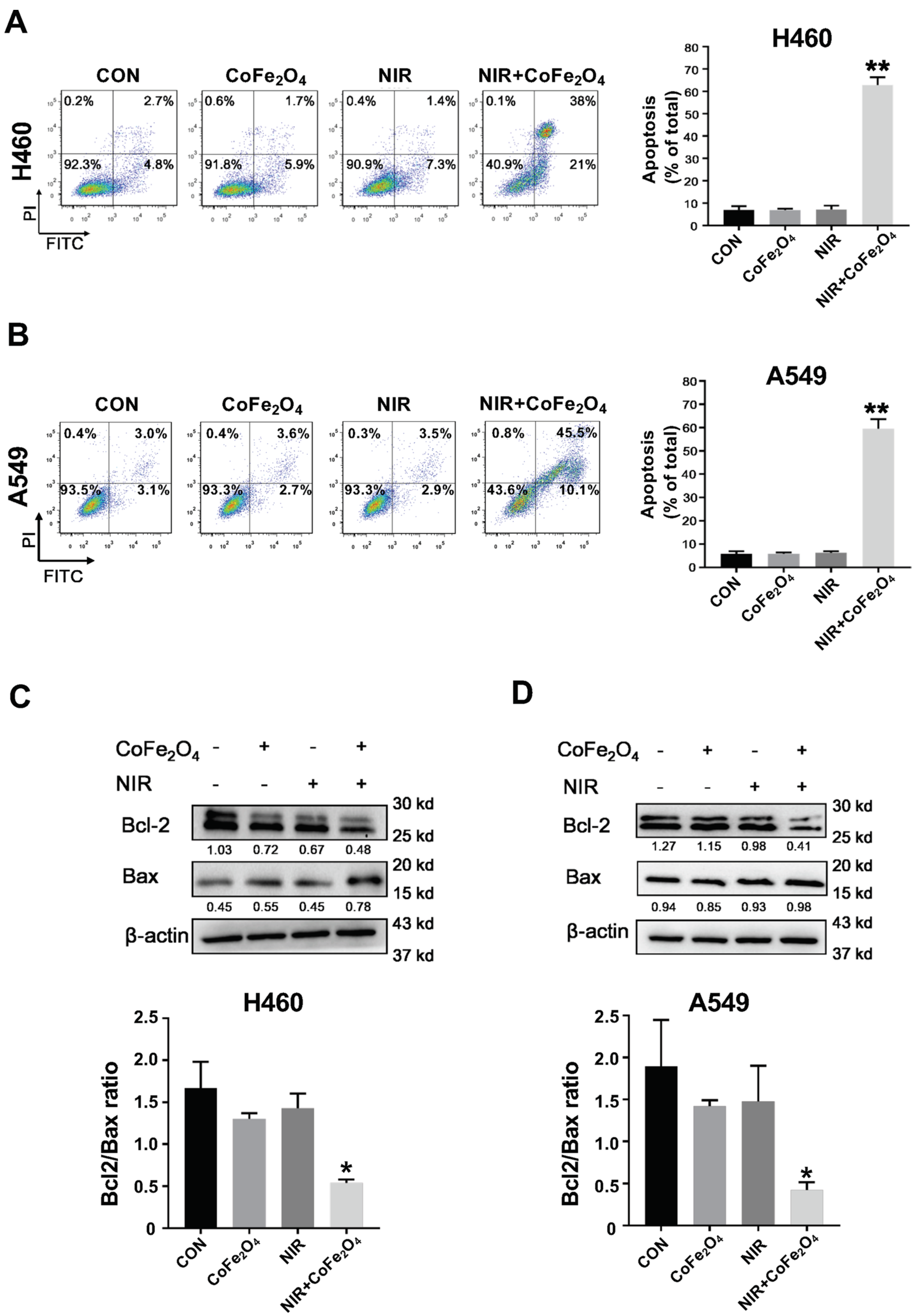

Fig. 4 (See legend on previous page.)

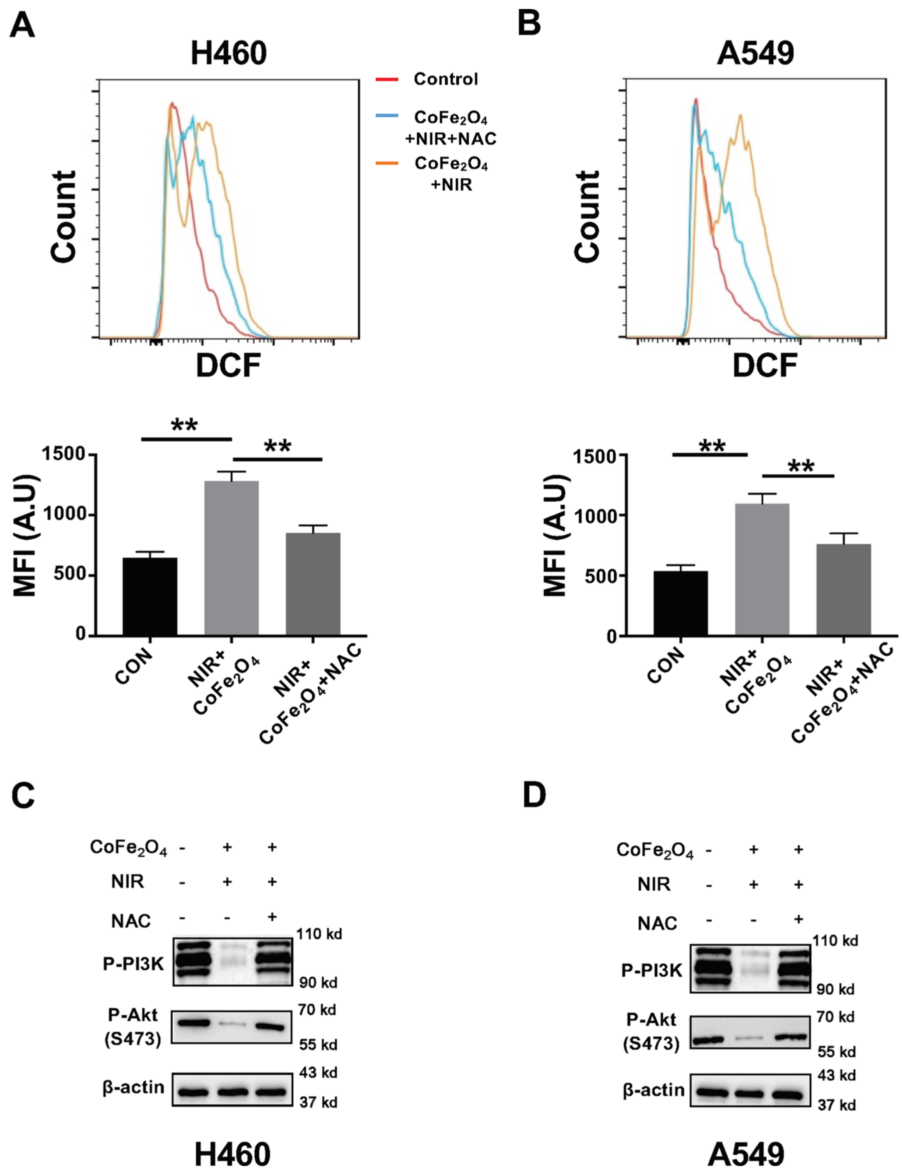

Fig. 5 The combination of $CoFe_2O_4$-QDs and NIR induces ROS generation through regulating PI3K/AKT pathway. **a**, **b** NCI-H460 and A549 NSCLCs were treated with the $CoFe_2O_4$-QDs and NIR laser with or without NAC for 5 min. The ROS level was detected by FACS and the mean fluorescent intensity was quantified, respectively. The data were shown as mean ± SD, $N = 3$. $^{**}P < 0.01$. **c**, **d** The protein level of *P*-PI3K and *P*-AKT was determined by Western blot analysis. Representative images are shown, $N = 3$

phosphorylated by PI3K and therefore inactivates the pro-apoptotic protein Bax and protects cells from apoptosis. In addition, phosphorylated AKT is also able to stabilize the MDM2/p53 complex, which regulates cell survival [50]. In this context, the role of such pathway in $CoFe_2O_4$-QDs induced ROS secretion was investigated. As expected, we found that excessive ROS caused by $CoFe_2O_4$-QDs significantly downregulated the expression of PI3K/AKT pathways and therefore cause tumor cell apoptosis via activating Bax but inactivating Bcl-2 protein. This finding was further confirmed by adding ROS inhibitor, which reversed the PI3K/AKT expression and decreased the production of ROS. Since PI3K/AKT pathway is known to regulate cell survival and death, especially in cancer cells, understanding such mechanisms of $CoFe_2O_4$-QDs in killing NSCLC would help us to develop more options for combinational therapies.

In summary, to develop novel photosensitizers for alternative tumor killing therapy, we successfully constructed $CoFe_2O_4$-QDs by using hydrothermal

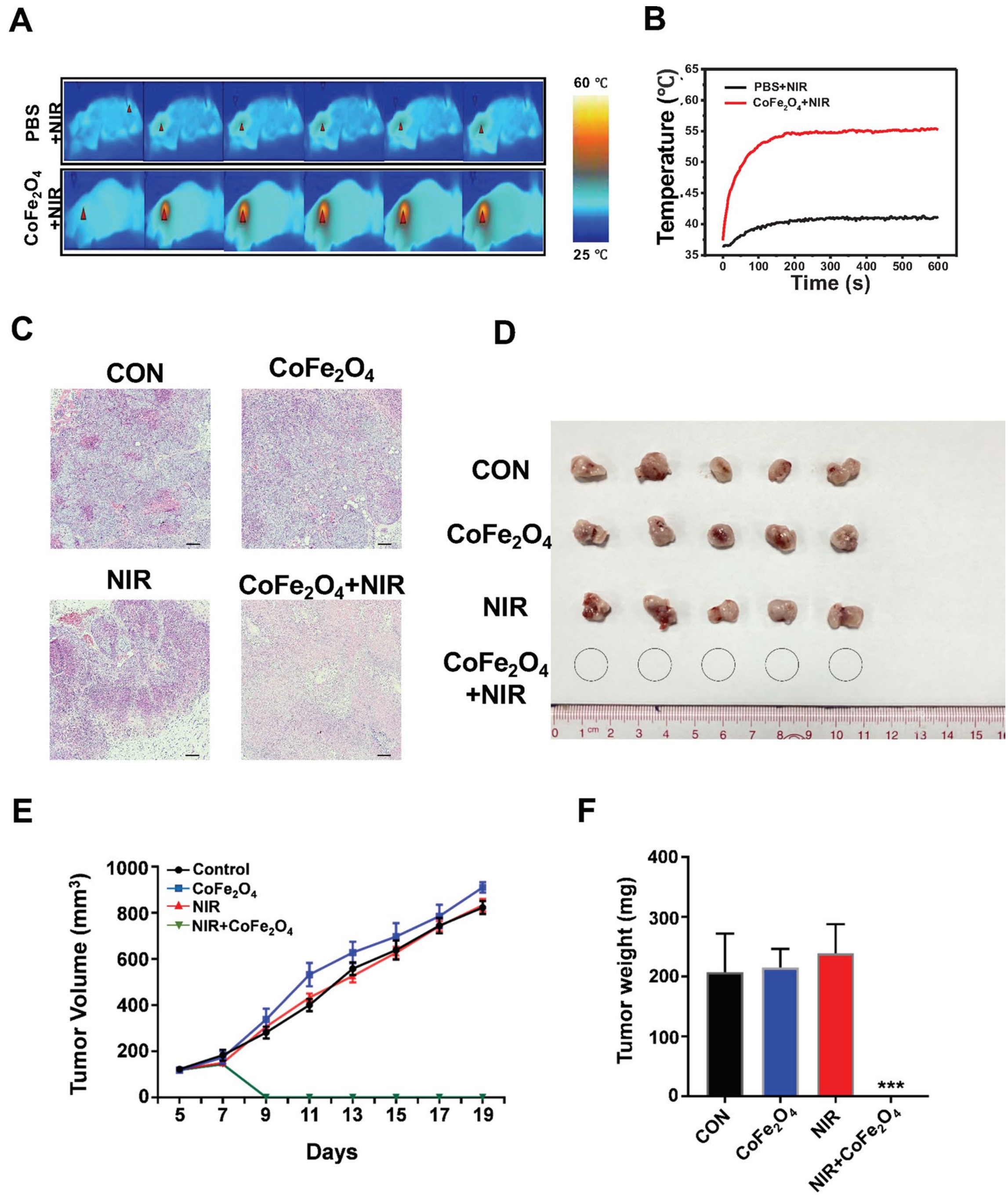

Fig. 6 In vivo tumor killing assessment of the combination of $CoFe_2O_4$-QDs and NIR treatment. **a** The representative infrared thermal images of M-NSG mice bearing NCI-H460 tumor xenografts are shown. **b** The temperature curve shows the increasing temperature within tumor xenografts under NIR irradiation. **c** H&E pathological staining of each group was photographed 1 day after treatment. Apparent necrosis could be observed in combination group. Representative images are shown, $N = 3$. **d** The photograph of the xenografts in each group after the mice were sacrificed, $N = 5$. **e**, **f** The growth curve and weight of tumor xenografts in each group was recorded. The data were shown as mean ± SD, $N = 5$. ***$P < 0.001$

approach in a low-cost and easy manner in this study. The $CoFe_2O_4$-QDs have a wide NIR absorbance, good biocompatibility and photothermal conversion ability. In addition, compared to previously reported QDs, $CoFe_2O_4$-QDs exhibited synergistic PTT/PDT effect in killing NSCLC tumors, which representing a promising multifunctional agent in further phototherapies of NSCLC. Moreover, with the NIR irradiation, $CoFe_2O_4$-QDs could kill NSCLC mainly through inducing ROS generation via regulating Bcl-2/Bax expression through the upstream PI3K/AKT signaling pathway. As for in vivo tumor killing ability, $CoFe_2O_4$-QDs combined with NIR could eliminate the NSCLC tumor xenografts completely without obvious toxic effects. These findings prove that $CoFe_2O_4$-QDs owns promising applications to be developed as a novel NSCLC killing reagent.

Conclusion

All in all, $CoFe_2O_4$-QDs we synthesized could exhibit superior PTT/PDT synergistic effects in suppressing NSCLC by inducing ROS generation through regulating PI3K/AKT pathway, which shed light to the mechanism research and applications of novel photosensitizers establishments.

Supplementary Information

The online version contains supplementary material available at https://doi.org/10.1186/s11671-021-03580-5.

Additional file 1: Supplementary Figure 1. In vitro ROS detection. Related to Fig. 5A and B. DCF FACS analysis shows the ROS level in NCI-H460 and A549 with diffrent treatments. Representative data are shown. N = 3 C and D. The protein level of P-PI3K and P-Akt were determined by WB. Reperesentative images are shown.

Additional file 2: Supplementary Figure 2. Related Fig. 6. A The Ki-67 IHC staining of tumer xenografts in each group 1 day after treatment. Reperesentative images are shown. Scale bar, 50 nm. N = 3. B The quantification of Ki-67 positive staining from IHC images. At least 10 frames (40X) were quantified. The data are shown as $\pm SD$. $^{**}P < 0.01$. C Reperesentative H&E staining of kidney, liver, lung, heart and spleen in control group and combinational treatment groups after mice were sacrificed. N = 5. Sacle bar, 50 nm.

Authors' contributions

JL, JC, ZW and QW designed the experiments. JL, XY, RZ, MZ and JH performed the experiments. JL and RZ analyzed the data. JL, JC, ZW and QW wrote the manuscript. All authors read and approved the final manuscript.

Funding

This study was supported by the National Natural Science Foundation of China (Nos. 81974253, 81901641), the Scientific Research Foundation of PEKING UNIVERSITY SHENZHEN HOSPITAL (KYQD202100X), the Nature Science Foundation of Guangdong Province (No. 2019A1515011112), Shenzhen Key Laboratory of Inflammatory and Immunology Diseases (No. ZDSYS20200811143756018), the Key Program for Basic Research of Shenzhen Science and Technology Innovation Commission (No. JCYJ20200109140203849), China Postdoctoral Science Foundation (No. 2021M693290) and Shenzhen Sanming Project of Shenzhen Municipal Health Commission (No. SZSM201612009).

Availability of data and materials

The data that support the findings of this study are available from the corresponding author upon reasonable request.

Declarations

Ethics approval and consent to participate

This study was approved by the ethics committee of Peking University Shenzhen Hospital.

Competing interest

The authors declared they have no competing interests.

Author details

[1]Department of Rheumatism and Immunology, Peking University Shenzhen Hospital, Shenzhen Peking University-The Hong Kong University of Science and Technology Medical Center, Shenzhen 518036, Guangdong, China. [2]Shenzhen Key Laboratory of Immunity and Inflammatory Diseases, Peking University Shenzhen Hospital, Shenzhen 518036, Guangdong, China. [3]Cardiovascular Hospital, No. 1 Hospital of Xi'an City, Xi'an 710002, China. [4]Cancer Research Institute, School of Basic Medical Sciences, Southern Medical University, Guangzhou 510515, Guangdong, China. [5]School of Advanced Materials and Nanotechnology, Xidian University, Xi'an 710126, China.

Received: 14 April 2021 Accepted: 21 July 2021
Published online: 28 July 2021

References

1. Sung H, Ferlay J, Siegel RL, Laversanne M, Soerjomataram I, Jemal A, Bray F (2021) Global cancer statistics 2020: GLOBOCAN estimates of incidence and mortality worldwide for 36 cancers in 185 countries. CA Cancer J Clin. https://doi.org/10.3322/caac.21660
2. Siegel RL, Miller KD, Fuchs HE (2021) Jemal A (2021) Cancer statistics. CA Cancer J Clin 71(1):7–33. https://doi.org/10.3322/caac.21654
3. Howlader N, Forjaz G, Mooradian MJ, Meza R, Kong CY, Cronin KA, Mariotto AB, Lowy DR, Feuer EJ (2020) The effect of advances in lung-cancer treatment on population mortality. N Engl J Med 383(7):640–649. https://doi.org/10.1056/NEJMoa1916623
4. Jee J, Li BT (2021) Expanding the nanotherapeutic toolbox for non-small-cell lung cancer. Ann Oncol Off J Eur Soc Med Oncol 32(1):9–11. https://doi.org/10.1016/j.annonc.2020.11.010
5. Guerra SL, Maertens O, Kuzmickas R, De Raedt T, Adeyemi RO, Guild CJ, Guillemette S, Redig AJ, Chambers ES, Xu M, Tiv H, Santagata S, Jänne PA, Elledge SJ, Cichowski K (2020) A deregulated HOX gene axis confers an epigenetic vulnerability in KRAS-mutant lung cancers. Cancer Cell 37(5):705-719.e706. https://doi.org/10.1016/j.ccell.2020.03.004
6. Harrison PT, Vyse S, Huang PH (2020) Rare epidermal growth factor receptor (EGFR) mutations in non-small cell lung cancer. Semin Cancer Biol 61:167–179. https://doi.org/10.1016/j.semcancer.2019.09.015
7. Liu WJ, Du Y, Wen R, Yang M, Xu J (2020) Drug resistance to targeted therapeutic strategies in non-small cell lung cancer. Pharmacol Therap 206:107438. https://doi.org/10.1016/j.pharmthera.2019.107438
8. Piotrowska Z, Hata AN (2020) Resistance to first-line osimertinib in EGFR-mutant NSCLC: tissue is the issue. Clin Cancer Res Off J Am Assoc Cancer Res 26(11):2441–2443. https://doi.org/10.1158/1078-0432.Ccr-20-0097
9. Urbanska EM, Sørensen JB, Santoni-Rugiu E (2020) Treatment algorithm for advanced ALK-rearranged NSCLC. J Thorac Oncol Off Publ Int Assoc Study Lung Cancer 15(9):e156–e157. https://doi.org/10.1016/j.jtho.2020.04.039
10. Camidge DR, Doebele RC, Kerr KM (2019) Comparing and contrasting predictive biomarkers for immunotherapy and targeted therapy of NSCLC. Nat Rev Clin Oncol 16(6):341–355. https://doi.org/10.1038/s41571-019-0173-9
11. Doroshow DB, Sanmamed MF, Hastings K, Politi K, Rimm DL, Chen L, Melero I, Schalper KA, Herbst RS (2019) Immunotherapy in non-small cell lung cancer: facts and hopes. Clin Cancer Res Off J Am Assoc Cancer Res 25(15):4592–4602. https://doi.org/10.1158/1078-0432.Ccr-18-1538
12. Uprety D, Mandrekar SJ, Wigle D, Roden AC, Adjei AA (2020) Neoadjuvant immunotherapy for NSCLC: current concepts and future approaches. J Thorac Oncol Off Publ Int Assoc Study Lung Cancer 15(8):1281–1297. https://doi.org/10.1016/j.jtho.2020.05.020

13. Rotow J, Bivona TG (2017) Understanding and targeting resistance mechanisms in NSCLC. Nat Rev Cancer 17(11):637–658. https://doi.org/10.1038/nrc.2017.84
14. Wu SG, Shih JY (2018) Management of acquired resistance to EGFR TKI-targeted therapy in advanced non-small cell lung cancer. Mol Cancer 17(1):38. https://doi.org/10.1186/s12943-018-0777-1
15. Hou YJ, Yang XX, Liu RQ, Zhao D, Guo CX, Zhu AC, Wen MN, Liu Z, Qu GF, Meng HX (2020) Pathological mechanism of photodynamic therapy and photothermal therapy based on nanoparticles. Int J Nanomed 15:6827–6838. https://doi.org/10.2147/ijn.S269321
16. Li W, Yang J, Luo L, Jiang M, Qin B, Yin H, Zhu C, Yuan X, Zhang J, Luo Z, Du Y, Li Q, Lou Y, Qiu Y, You J (2019) Targeting photodynamic and photothermal therapy to the endoplasmic reticulum enhances immunogenic cancer cell death. Nat Commun 10(1):3349. https://doi.org/10.1038/s41467-019-11269-8
17. Sun Y, Zhang Y, Gao Y, Wang P, He G, Blum NT, Lin J, Liu Q, Wang X, Huang P (2020) Six birds with one stone: versatile nanoporphyrin for single-laser-triggered synergistic phototheranostics and robust immune activation. Adv Mater (Deerfield Beach, Fla) 32(48):e2004481. https://doi.org/10.1002/adma.202004481
18. Wang P, Sun S, Ma H, Sun S, Zhao D, Wang S, Liang X (2020) Treating tumors with minimally invasive therapy: a review. Mater Sci Eng C Mater Biol Appl 108:110198. https://doi.org/10.1016/j.msec.2019.110198
19. Kim JY, Choi WI, Kim M, Tae G (2013) Tumor-targeting nanogel that can function independently for both photodynamic and photothermal therapy and its synergy from the procedure of PDT followed by PTT. J Control Release Off J Control Release Soc 171(2):113–121. https://doi.org/10.1016/j.jconrel.2013.07.006
20. Mou J, Lin T, Huang F, Chen H, Shi J (2016) Black titania-based theranostic nanoplatform for single NIR laser induced dual-modal imaging-guided PTT/PDT. Biomaterials 84:13–24. https://doi.org/10.1016/j.biomaterials.2016.01.009
21. Hou X, Tao Y, Pang Y, Li X, Jiang G, Liu Y (2018) Nanoparticle-based photothermal and photodynamic immunotherapy for tumor treatment. Int J Cancer 143(12):3050–3060. https://doi.org/10.1002/ijc.31717
22. Zaharie-Butucel D, Potara M, Suarasan S, Licarete E, Astilean S (2019) Efficient combined near-infrared-triggered therapy: phototherapy over chemotherapy in chitosan-reduced graphene oxide-IR820 dye-doxorubicin nanoplatforms. J Colloid Interface Sci 552:218–229. https://doi.org/10.1016/j.jcis.2019.05.050
23. Wang J, Wu X, Shen P, Wang J, Shen Y, Shen Y, Webster TJ, Deng J (2020) Applications of inorganic nanomaterials in photothermal therapy based on combinational cancer treatment. Int J Nanomed 15:1903–1914. https://doi.org/10.2147/ijn.S239751
24. Chilakamarthi U, Giribabu L (2017) Photodynamic therapy: past, present and future. Chem Rec (New York, NY) 17(8):775–802. https://doi.org/10.1002/tcr.201600121
25. Vankayala R, Hwang KC (2018) Near-infrared-light-activatable nanomaterial-mediated phototheranostic nanomedicines: an emerging paradigm for cancer treatment. Adv Mater (Deerfield Beach, Fla) 30(23):e1706320. https://doi.org/10.1002/adma.201706320
26. Albert K, Hsu HY (2016) Carbon-based materials for photo-triggered theranostic applications. Molecules (Basel, Switzerland). https://doi.org/10.3390/molecules21111585
27. Lee HP, Gaharwar AK (2020) Light-responsive inorganic biomaterials for biomedical applications. Adv Sci 7(17):2000863. https://doi.org/10.1002/advs.202000863
28. Gaio E, Conte C, Esposito D, Reddi E, Quaglia F, Moret F (2020) CD44 targeting mediated by polymeric nanoparticles and combination of chlorine TPCS(2a)-PDT and docetaxel-chemotherapy for efficient killing of breast differentiated and stem cancer cells in vitro. Cancers. https://doi.org/10.3390/cancers12020278
29. Samia AC, Chen X, Burda C (2003) Semiconductor quantum dots for photodynamic therapy. J Am Chem Soc 125(51):15736–15737. https://doi.org/10.1021/ja0386905
30. Fan HY, Yu XH, Wang K, Yin YJ, Tang YJ, Tang YL, Liang XH (2019) Graphene quantum dots (GQDs)-based nanomaterials for improving photodynamic therapy in cancer treatment. Eur J Med Chem 182:111620. https://doi.org/10.1016/j.ejmech.2019.111620
31. Juzenas P, Chen W, Sun YP, Coelho MA, Generalov R, Generalova N, Christensen IL (2008) Quantum dots and nanoparticles for photodynamic and radiation therapies of cancer. Adv Drug Deliv Rev 60(15):1600–1614. https://doi.org/10.1016/j.addr.2008.08.004
32. Biju V, Mundayoor S, Omkumar RV, Anas A, Ishikawa M (2010) Bioconjugated quantum dots for cancer research: present status, prospects and remaining issues. Biotechnol Adv 28(2):199–213. https://doi.org/10.1016/j.biotechadv.2009.11.007
33. McHugh KJ, Jing L, Behrens AM, Jayawardena S, Tang W, Gao M, Langer R, Jaklenec A (2018) Biocompatible semiconductor quantum dots as cancer imaging agents. Adv Mater (Deerfield Beach, Fla) 30(18):e1706356. https://doi.org/10.1002/adma.201706356
34. Meng HM, Zhao D, Li N, Chang J (2018) A graphene quantum dot-based multifunctional two-photon nanoprobe for the detection and imaging of intracellular glutathione and enhanced photodynamic therapy. Analyst 143(20):4967–4973. https://doi.org/10.1039/c8an00677f
35. Kuo WS, Shao YT, Huang KS, Chou TM, Yang CH (2018) Antimicrobial amino-functionalized nitrogen-doped graphene quantum dots for eliminating multidrug-resistant species in dual-modality photodynamic therapy and bioimaging under two-photon excitation. ACS Appl Mater Interfaces 10(17):14438–14446. https://doi.org/10.1021/acsami.8b01429
36. Yuan M, Xu S, Zhang Q, Zhao B, Feng B, Ji K, Yu L, Chen W, Hou M, Xu Y, Fu X (2020) Bicompatible porous Co_3O_4 nanoplates with intrinsic tumor metastasis inhibition for multimodal imaging and DNA damage–mediated tumor synergetic photothermal/photodynamic therapy. Chem Eng J. https://doi.org/10.1016/j.cej.2020.124874
37. Chen J, Zhang R, Tao C, Huang X, Chen Z, Li X, Zhou J, Zeng Q, Zhao B, Yuan M, Ma M, Wu Z (2020) CuS-NiS(2) nanomaterials for MRI guided phototherapy of gastric carcinoma via triggering mitochondria-mediated apoptosis and MLKL/CAPG-mediated necroptosis. Nanotoxicology 14(6):774–787. https://doi.org/10.1080/17435390.2020.1759727
38. Kargar A, Yavuz S, Kim TK, Liu CH, Kuru C, Rustomji CS, Jin S, Bandaru PR (2015) Solution-processed $CoFe_2O_4$ nanoparticles on 3D carbon fiber papers for durable oxygen evolution reaction. ACS Appl Mater Interfaces 7(32):17851–17856. https://doi.org/10.1021/acsami.5b04270
39. Indra A, Menezes PW, Sahraie NR, Bergmann A, Das C, Tallarida M, Schmeißer D, Strasser P, Driess M (2014) Unification of catalytic water oxidation and oxygen reduction reactions: amorphous beat crystalline cobalt iron oxides. J Am Chem Soc 136(50):17530–17536. https://doi.org/10.1021/ja509348t
40. Yin XM, Oltvai ZN, Korsmeyer SJ (1994) BH1 and BH2 domains of Bcl-2 are required for inhibition of apoptosis and heterodimerization with Bax. Nature 369(6478):321–323. https://doi.org/10.1038/369321a0
41. Vansteenkiste J, Wauters E, Reymen B, Ackermann CJ, Peters S, De Ruysscher D (2019) Current status of immune checkpoint inhibition in early-stage NSCLC. Ann Oncol Off J Eur Soc Med Oncol 30(8):1244–1253. https://doi.org/10.1093/annonc/mdz175
42. Gelatti ACZ, Drilon A, Santini FC (2019) Optimizing the sequencing of tyrosine kinase inhibitors (TKIs) in epidermal growth factor receptor (EGFR) mutation-positive non-small cell lung cancer (NSCLC). Lung Cancer (Amst, Neth) 137:113–122. https://doi.org/10.1016/j.lungcan.2019.09.017
43. Zuber G, Weiss E, Chiper M (2019) Biocompatible gold nanoclusters: synthetic strategies and biomedical prospects. Nanotechnology 30(35):352001. https://doi.org/10.1088/1361-6528/ab2088
44. Wang X, Li X, Mao Y, Wang D, Zhao Q, Wang S (2019) Multi-stimuli responsive nanosystem modified by tumor-targeted carbon dots for chemo-phototherapy synergistic therapy. J Colloid Interface Sci 552:639–650. https://doi.org/10.1016/j.jcis.2019.05.085
45. Cai G, Yu Z, Tong P, Tang D (2019) Ti(3)C(2) MXene quantum dot-encapsulated liposomes for photothermal immunoassays using a portable near-infrared imaging camera on a smartphone. Nanoscale 11(33):15659–15667. https://doi.org/10.1039/c9nr05797h
46. Lien EC, Dibble CC, Toker A (2017) PI3K signaling in cancer: beyond AKT. Curr Opin Cell Biol 45:62–71. https://doi.org/10.1016/j.ceb.2017.02.007
47. Fresno Vara JA, Casado E, de Castro J, Cejas P, Belda-Iniesta C, González-Barón M (2004) PI3K/Akt signalling pathway and cancer. Cancer Treat Rev 30(2):193–204. https://doi.org/10.1016/j.ctrv.2003.07.007
48. Wen C, Wang H, Wu X, He L, Zhou Q, Wang F, Chen S, Huang L, Chen J, Wang H, Ye W, Li W, Yang X, Liu H, Peng J (2019) ROS-mediated inactivation of the PI3K/AKT pathway is involved in the antigastric cancer effects of thioredoxin reductase-1 inhibitor chaetocin. Cell Death Dis 10(11):809. https://doi.org/10.1038/s41419-019-2035-x

49. Su X, Shen Z, Yang Q, Sui F, Pu J, Ma J, Ma S, Yao D, Ji M, Hou P (2019) Vitamin C kills thyroid cancer cells through ROS-dependent inhibition of MAPK/ERK and PI3K/AKT pathways via distinct mechanisms. Theranostics 9(15):4461–4473. https://doi.org/10.7150/thno.35219
50. Abraham AG, O'Neill E (2014) PI3K/Akt-mediated regulation of p53 in cancer. Biochem Soc Trans 42(4):798–803. https://doi.org/10.1042/bst20140070

Publisher's Note

Springer Nature remains neutral with regard to jurisdictional claims in published maps and institutional affiliations.